Saudi Journal of Biological Sciences (2017) **24**, 410–420

King Saud University

Saudi Journal of Biological Sciences

www.ksu.edu.sa
www.sciencedirect.com

ORIGINAL ARTICLE

Estimation of gross primary production of irrigated maize using Landsat-8 imagery and Eddy Covariance data

Rangaswamy Madugundu [a,*], Khalid A. Al-Gaadi [a,b], ElKamil Tola [a], Ahmed G. Kayad [b], Chandra Sekhar Jha [c]

[a] *Precision Agriculture Research Chair, King Saud University, Riyadh, Saudi Arabia*
[b] *Department of Agricultural Engineering, College of Food and Agriculture Sciences, King Saud University, Riyadh, Saudi Arabia*
[c] *Forestry and Ecology Group, National Remote Sensing Center, Indian Space Research Organization, Hyderabad, India*

Received 18 May 2016; revised 4 September 2016; accepted 2 October 2016
Available online 8 October 2016

KEYWORDS

Carbon flux;
Remote sensing;
Eddy covariance;
Maize crop

Abstract A study was conducted to understand the potential of Landsat-8 in the estimation of gross primary production (GPP) and to quantify the productivity of maize crop cultivated under hyper-arid conditions of Saudi Arabia. The GPP of maize crop was estimated by using the Vegetation Photosynthesis Model (VPM) utilizing remote sensing data from Landsat-8 reflectance (GPP_{VPM}) as well as the meteorological data provided by Eddy Covariance (EC) system (GPP_{EC}), for the period from August to November 2015. Results revealed that the cumulative GPP_{EC} for the entire growth period of maize crop was 1871 g C m^{-2}. However, the cumulative GPP determined as a function of the enhanced vegetation index – EVI (GPP_{EVI}) was 1979 g C m^{-2}, and that determined as a function of the normalized difference vegetation index – NDVI (GPP_{NDVI}) was 1754 g C m^{-2}. These results indicated that the GPP_{EVI} was significantly higher than the GPP_{EC} (R^2 = 0.96, P = 0.0241 and RMSE = 12.6%). While, the GPP_{NDVI} was significantly lower than the GPP_{EC} (R^2 = 0.93, P = 0.0384 and RMSE = 19.7%). However, the recorded relative error between the GPP_{EC} and both the GPP_{EVI} and the GPP_{NDVI} was −6.22% and 5.76%, respectively. These results demonstrated the potential of the landsat-8 driven VPM model for the estimation of GPP, which is relevant to the productivity and carbon fluxes.

* Corresponding author.
E-mail address: rmadugundu@ksu.edu.sa (R. Madugundu).
Peer review under responsibility of King Saud University.

ELSEVIER Production and hosting by Elsevier

1. Introduction

The gross primary production (GPP) is a critical parameter for carbon cycle and climate research. It is used to quantify the total amount of energy or biomass produced by vegetation through photosynthesis over a unit of time (Pingintha et al.,

http://dx.doi.org/10.1016/j.sjbs.2016.10.003
1319-562X

2010; Vashum and Jayakumar, 2012). Along with forest lands, agricultural ecosystems are also considered as one of the major contributors in carbon sequestration and mitigating the effects of the global climatic change. Hence, quantitative estimates of the spatial and temporal distribution of the GPP from agriculture fields is one the important factors in monitoring carbon exchange over a region (Gitelson et al., 2008). In agro-ecosystem studies, information on the GPP of croplands is essential for monitoring and assessing the variations in productivity and subsequently those can be used in optimizing the agricultural management practices (Baker and Griffis, 2005; Falge et al., 2002; Wagle et al., 2015).

Since the 1990s, Eddy Covariance (EC) technique, a key atmospheric measurement technique to measure and calculate vertical turbulent fluxes within atmospheric boundary layers, is being considered as one of the best micrometeorological methods for the estimation of CO_2 and H_2O fluxes and as a primary source of data for the development and validation of satellite-based GPP models (Li et al., 2007; Shim et al., 2014). The GPP can be estimated using both EC recorded data and satellite images (Hunt et al., 2004; Sakamoto et al., 2011). The EC system records the fluxes at high frequency (10–20 Hz) over an ecosystem based on the wind speed and direction. The details of EC system and the principle of footprint and data analysis was provided in Goulden et al. (1997), Falge et al. (2002), Osmond et al. (2004) and Wagle et al. (2015).

Remotely sensed estimates of terrestrial primary production have evolved significantly over the past few decades, and the resulting datasets provide necessary information about the emission of CO_2 into the atmosphere (Pan et al., 2014). Due to the high spatial variability, measurement of CO_2 and water fluxes over large areas is very challenging. However, advances in satellite remote sensing (RS) observations provide consistent spatially fine-scale estimates and facilitate the monitoring process of the Net Ecosystem Exchange (NEE) at larger scales (DeFries, 2008; Zhao and Running, 2010). Satellite RS can provide consistent and systematic estimates of GPP and NEE at the field and regional levels, relying on Light Use Efficiency (LUE) based model simulation. The Landsat satellite has the advantage of large coverage, high spatial resolution (i.e. 30 m) with 16-day temporal resolution and free access to the data; hence it is being widely used in most of the studies conducted for the estimation of GPP (Silva et al., 2013; Victor et al., 2015). On the other hand, vegetation indices such as Normalized Differential Vegetation Index-NDVI (Tucker, 1979), the Enhanced Vegetation Index-EVI (Huete et al., 1997, 2002) and the Land Surface Water Index-LSWI (Xiao et al., 2004a, 2005a) are widely used for the estimation GPP.

LUE-based Vegetation Photosynthesis Model (VPM) has been widely used for the estimation of the GPP and the Net Primary Production (NPP). For example, it was used for studies in grasslands (Li et al., 2007; Wu et al., 2008), forests (Xiao et al., 2004a, 2005a,b) and croplands or agriculture fields (Wang et al., 2010; Yan et al., 2009). The GPP calculated from the EC flux towers (GPP_{EC}) is widely utilized for the validation of GPP estimates from satellite-based models, such as Vegetation Photosynthesis Model-VPM (Wu et al., 2010; Sakamoto et al., 2011; Tang et al., 2015).

In Saudi Arabia, most of the agricultural area is confined to fodder crops such as alfalfa, Rhodes grass, maize, etc., cultivated under center pivot irrigation systems. Due to the high evaporation during summer months, almost all crops suffer from drought stress. Maize crop, which considered as one of the most important forage crops in Saudi Arabia, is cultivated both in spring and summer seasons. Based on the fact that maize crop has a C_4 pathway of photosynthesis, it is capable of using water and carbon dioxide more efficiently. The present study was conducted to understand the potential of Landsat-8 in the estimation of the GPP and to quantify the productivity of maize crop grown under hyper-arid conditions of Saudi Arabia. The objectives of this study were: (i) to assess the capabilities of Landsat-8 derived vegetation indices in the estimation of the GPP, (ii) to explore the EC measured CO_2 fluxes for the estimation of the GPP and (iii) to compare the VPM model estimated GPP (GPP_{VPM}) with the EC estimated GPP (GPP_{EC}).

2. Materials and methods

2.1. Study area

This study was conducted on a 50 ha maize field under center pivot irrigation system in Todhia Arable Farm (TAF). The farm is located with-in the latitudes of 24°10′22.77″ and 24°12′37.25″N and the longitudes of 47°56′14.60″ and 48°05′08.56″ E, between Al-Kharj and Haradh cities in the Eastern Region of Saudi Arabia (Fig. 1). The climate of the study area was hyper-arid with hot summers (40 ± 2 °C) and cold to moderate winters (15 ± 3 °C). The annual rainfall was about 90 mm; most of which occurred in the period November to February. The major crops cultivated in the study area were forages (alfalfa, Rhodes grass, corn, etc.) and vegetable crops (carrot, onion, etc.). Furthermore, most of the water used for irrigating agricultural fields is from groundwater through the bore wells.

2.2. Biophysical parameters – maize crop

Maize crop, sown on August 18, 2015 was cultivated for silage/fodder purpose (forage maize) and was harvested at the physiological maturity stage (i.e. 85 days after sowing – DAS). The total amount of the applied irrigation water was 1163 mm. To understand the nature of the crop, *in-situ* biophysical parameters such as leaf area index (LAI), stomatal conductance, chlorophyll content and gas exchange measurements were recorded. LAI was determined by collecting five readings from each sampled location with the plant canopy analyzer (LAI-2200). The leaf chlorophyll content was recorded using a Chlorophyll Meter (SPAD-502). While measuring the leaf chlorophyll content, three SPAD readings per leaf were collected from the most recently collared leaf of the plant. Consequently, gas exchange measurements – the rate of photosynthesis (P_n), transpiration (ER), stomatal conductance (gs) and intercellular CO_2 concentration (C_i) were measured, for the assessment of photosynthetic assimilation of CO_2, using a portable photosynthesis system (LI-6400XT).

2.3. Meteorological and Flux measurements

The Eddy Covariance (EC) flux tower was established in May 2013 on a selected center pivot irrigated 50 ha field (24° 10′

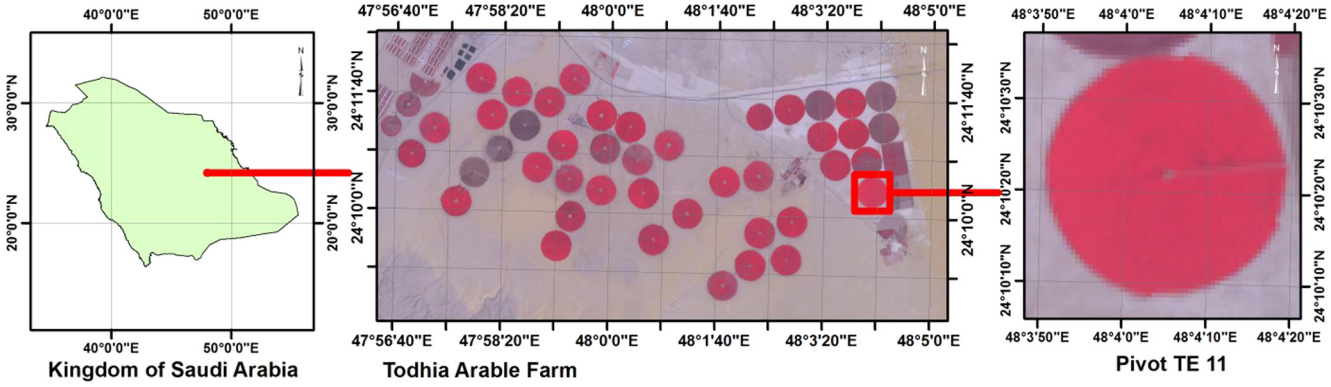

Figure 1 Location map of the experimental site (Pivot TE 11), Todhia Arable Farm.

38.55″ N, 48° 04′ 3.77″ E). The EC system consists of an ultrasonic anemometer (Windmaster Pro, GILL) and an open path CO_2/H_2O analyzer (Li-7500, Li-Cor), which continuously measure CO_2, H_2O and energy fluxes at a frequency of 10 Hz. The measuring height of the EC system was 3.45 m. Flux densities of CO_2, sensible heat, latent heat and water vapor fluxes were measured and aggregated to an average time of 30 min, from the EC collected 10 Hz time series raw data. Because of the instrument malfunction, variation in weather condition, and calibration issues; high-quality data comprised 72% to 81% of the data, collected during the maize crop growth period, was used for this study. Gap filling was carried out where missing or bad quality data were observed. In which, a linear interpolation method was used for small blocks of missing or bad quality data (i.e. less than few hours). While, larger gaps were treated with the mean diurnal ensemble values (Falge et al., 2002). Finally, the data were rejected when it was recorded while the winds were not coming from the experimental field, or at the time of rain and when the irrigation system passed through the upwind fetch as described in Baldocchi and Meyers (1998).

2.4. Landsat-8 imagery and vegetation indices

The Landsat-8 satellite is working with two instruments namely, the Operational Land Imager (OLI) and the Thermal Infrared Sensor (TIRS). OLI consists of a multispectral (visible, NIR and SWIR) sensor with a spatial resolution of 30 m, and panchromatic with 15 m spatial resolution. While, the spatial resolution of the thermal sensor is 100 m. Out of the 11 spectral bands of Landsat-8 (OLI), five bands, namely, the blue (452–512 nm), the green (533–590 nm), the Red (636–673 nm), the near infrared (NIR: 851–879 nm) and the shortwave infrared (SWIR1: 1566–1651 nm and SWIR2: 2107–2294 nm) were designated for vegetation and land surfaces studies. The cloud free Landsat-8 images were downloaded from the datasets archived and freely accessible to the public from the US Geological Survey through Earth Explorer website (http://earthexplorer.usgs.gov).

In this study, 11 Landsat-8 images (level-1 geo tiff data products) were downloaded for the period from August to November 2015 (Table 1) and corrected for land surface reflectance (USGS, 2015). The pixels corresponding to the EC system footprint area (i.e. 400 m × 400 m) were extracted (15 × 15 pixels of 30 m × 30 m each) and were used for the assessment of vegetation indices and VPM model simulation (Kalfas et al., 2011; Souza et al., 2014; Victor et al., 2015; Kang et al., 2016).

Surface reflectance values from Landsat-8 spectral bands (blue, red, NIR and SWIR1) were calculated using header files and used to generate three vegetation indices, namely, the NDVI (Tucker, 1979), the EVI (Huete et al., 1997, 2002) and the LSWI (Xiao et al., 2004a, 2005a), using Eq. (1–3). Consequently, these indices were tested individually for the determination of maize GPP (Xiao et al., 2005c; Gwathmey et al., 2010; Sims et al., 2008).

$$\mathrm{NDVI} = (\rho_{\mathrm{nir}} - \rho_{\mathrm{red}})/(\rho_{\mathrm{nir}} + \rho_{\mathrm{red}}) \quad (1)$$

$$\mathrm{EVI} = 2.5\frac{\rho_{\mathrm{nir}} - \rho_{\mathrm{red}}}{[\rho_{\mathrm{nir}} + (6\rho_{\mathrm{red}}) - (7.5\rho_{\mathrm{blue}}) + 1]} \quad (2)$$

$$\mathrm{LSWI} = (\rho_{\mathrm{nir}} - \rho_{\mathrm{swir1}})/(\rho_{\mathrm{nir}} + \rho_{swir}1) \quad (3)$$

where ρ_{nir}, ρ_{red}, ρ_{swir}, ρ_{blue} are reflectances of the near infrared, red, shortwave infrared and blue bands of Landsat-8, respectively.

2.5. Gross primary production measured by Eddy Covariance Method (GPP_{EC})

The GPP measured by the EC system (GPP_{EC}) was calculated by Eq. (4) according to Wohlfahrt et al. (2005). The NEE of maize crop was estimated using the EC system measured CO_2 flux and meteorological data. The nighttime NEE was assumed to be equal to the ecosystem respiration (ER); while, the daytime NEE equal to the difference between the GPP and the daytime ER estimated using the function established for the nighttime NEE and environmental factors (e.g. air temperature, soil temperature, and soil moisture) as described by Desai et al. (2008). The half-hourly CO_2 flux data and the Photosynthetically Active Radiation (PAR) values ($< 5\ \mu\mathrm{mol\ m^{-2}\ s^{-1}}$) were used as the nighttime NEE. As a result, NEE data were divided into a daytime NEE and nighttime NEE. The daytime ecosystem respiration (R_{day}) was determined from the relationship between the nocturnal ecosystem respiration and air temperature (at 2 m height) using the Van't-Hoff function, as described by Wang et al. (2010).

$$GPP_{EC} = ER - NEE \quad (4)$$

where NEE is the net ecosystem exchange ($\mathrm{g\ C\ m^{-2}\ d^{-1}}$) and ER is the ecosystem respiration ($\mathrm{g\ C\ m^{-2}\ d^{-1}}$).

Table 1 Details of Landsat-8 images and the corresponding growth stages of the maize crop.

Path/ Row	Date of pass	DOY	Revisit (days)*	Crop age (days)	Growth stage
164/43	21 August15	233	–	–	Planting (V0)
165/43	28 August 15	240	7	2	Emergence (V1)
164/43	6 September 15	249	9	11	2 leaves (V2)
165/43	13 September 15	256	7	18	3–4 leaves (V4)
164/43	22 September 15	265	9	27	4–5 leaves (V5)
165/43	29 September 15	272	7	34	6–7 leaves (V7)
164/43	8 October 15	281	9	43	9–10 leaves (V10)
165/43	15 October 15	288	7	50	12 leaves (V12)
164/43	24 October 15	297	9	59	16 leaves (V16)
165/43	31 October 15	304	7	66	Silking/pollination (R1)
164/43	9 November 15	313	9	75	Milking stage (R2)

* Since the study site covered in two paths (i.e. 164 and 165), the revisit of Landsat-8 satellite was 7 and 9 days instead of 16.

For each growth stage, nighttime NEE values were regressed against the EC measured air temperature using Eq. (5). Subsequently, the GPP was estimated as NEE minus ER_{day} (Xiao et al., 2004a), and the GPP was calculated according to the nearest Landsat-8 date of pass (DOP) to ensure the consistency in the temporal assessment. In this study, the carbon uptake period (CUP) was determined as the number of days when the maize crop was a net sink of carbon (i.e. negative NEE) as described in Wagle et al. (2015). For the determination of the crop growth stage wise NEE and GPP, the acquired fluxes were summed for the phenological periods of the maize crop.

$$NEE_{night} = R_{ref,10} \times Q_{10}^{(T-10)/10} \quad (5)$$

where NEE_{night} is the nighttime NEE (g C m^{-2} s^{-1}); $R_{ref,10}$ is the respiration rate (g C m^{-2} s^{-1}) at 10 °C; Q_{10} (dimensionless) is the change in the rate of respiration with temperature; T is the soil temperature (°C).

2.6. GPP estimated by Vegetation Photosynthesis Model (VPM)

As described by Xiao et al. (2004a,b), the GPP was calculated (Eq. (6)) using the Vegetation Photosynthesis Model (VPM) as a function of the Photosynthetically Active Radiation (PAR), light use efficiency ε_g and the fraction of photosynthetically active radiation (FPAR) by chlorophyll in the vegetation canopy ($FPAR_{chl}$). The FPAR and the GPP were also calculated from Landsat-8 reflectance data using the EVI ($FPAR_{EVI}$) and NDVI ($FPAR_{NDVI}$) vegetation indices.

$$GPP_{VPM} = \varepsilon_g.FPAR_{chl}.PAR \quad (6)$$

The $FPAR_{EVI}$ (Eq. (7)) was calculated as a linear function of EVI, and the coefficient α (Xiao et al., 2004a), and the $FPAR_{NDVI}$ was computed (Eq. (8)) as a linear relation with NDVI (Asrar et al., 1992). In this study, α was set to 1.0 for the execution of VPM model as described in previous studies (Xiao et al. 2004a; Wu et al., 2008; Yan et al., 2009; Wang et al., 2010).

$$FPAR_{EVI} = \alpha.EVI \quad (7)$$

$$FPAR_{NDVI} = -0.168 + 1.24XNDVI \quad (8)$$

The light use efficiency (ε_g), was estimated (Eq. (9)) as a function of the apparent quantum yield or maximum light use efficiency (ε_0) and down-regulation factors (T_{scalar}, W_{scalar}, P_{scalar}) for the effects of temperature, soil water content and leaf phenology on the light use efficiency of vegetation, respectively (Wang et al., 2010); and is ranging between 0.0 and 1.0. Consequently, the scalar factors, T_{scalar} (Eq. (10)), W_{scalar} (Eq. (11)) and P_{scalar} (Eq. (12)) were computed.

$$\varepsilon_g = \varepsilon_0.T_{scalar}.W_{scalar}.P_{scalar} \quad (9)$$

$$T_{scalar} = \frac{(T - T_{min})(T - T_{max})}{[(T - T_{min})(T - T_{max})] - (T - T_{opt})^2} \quad (10)$$

where T_{scalar} represents the effects of temperature on the canopy photosynthesis (Raich et al., 1991); T_{min}, T_{max}, and T_{opt} are the minimum, maximum and optimum temperatures for photosynthetic activities, respectively. When the air temperatures fall below T_{min}, the T_{scalar} is assumed as zero (Xiao et al., 2004a,b).

In addition, the T_{min}, T_{opt}, and T_{max} parameters vary depending on the photosynthetic pathway (e.g., C3 vs. C4) and on the crop type. Due to changes in season, altitude and the diurnal cycle, consideration of T_{opt} is a difficult task. However, choosing a broad temperature range widely applicable to various cases prevents models from becoming plant-, specie-, or canopy-height specific (Kalfas et al., 2011). Hence, depending on the temperature ranges and the predominant climate, the T_{opt} parameter value was considered as 28 °C as described in earlier studies (Crafts-Brandner and Salvucci, 2002; Kim et al., 2007).

$$W_{scalar} = \frac{1 + LSWI}{1 + LSWI_{max}} \quad (11)$$

where $LSWI_{max}$ is the maximum LSWI across the growing season of the maize crop, which depends on the remote sensing data (Xiao et al., 2004b, 2005a). The LSWI ($\geqslant -0.1$) accounts for the DOY between 256 and 297. The obtained W_{scalar} for the studied maize crop was 0.34.

P_{scalar} accounts for the effects of leaf age on canopy photosynthesis (Xiao et al., 2004a). Maize phenology is divided into a vegetative stage and a reproductive stage (Yan et al., 2009). A clear-cut leaf expansion phase can be observed throughout the vegetative stage, but not in the reproductive stage. Hence, this study followed Yan's method (Yan et al., 2009) in calculat-

ing P_{scalar} for maize as a linear function of LSWI from emergence to full leaf expansion (Eq. (12)), as described by Wang et al. (2010, 2012).

$$P_{scalar} = \frac{1 + LSWI}{2} \quad (12)$$

The ε_0, apparent quantum yield was estimated using a non-linear hyperbolic function proposed to Michaelis–Menten (Eq. (13)) obtained from the NEE analysis of CO_2 and the PAR measured at EC flux tower site over a period of time (e.g., 1–2 weeks long) within the peak of the plant growing season (Yan et al., 2009; Wang et al., 2010).

$$NEE = \frac{\varepsilon_0.PAR.GPP_{max}}{\varepsilon_0.PAR + GPP_{max}} - ER \quad (13)$$

where NEE is the net ecosystem exchange measured by the EC system (g C m^{-2} d^{-1}), PAR is the photosynthetic active radiation measured in the flux tower, GPP_{max} is the maximum estimated GPP from flux data at a maximum photosynthetic capacity and ER is the ecosystem respiration measured by the EC system. In this study, the daytime NEE and PAR were measured within the peak period of vegetation growing season (V5 to V12) of the maize crop. The obtained ε_0 value was 0.61 g C mol PAR^{-1}.

2.7. Statistical analysis

The values of EVI, NDVI and LSWI, calculated from Landsat-8 reflectance, were averaged for the 225 pixels covering the surrounding area of the flux tower, and only pixels with highest quality assurance (QA) metrics were used. The root mean square error "RMSE," the relative error "RE" and the correlation coefficient were used to evaluate the performance of the GPP estimated by the VPM using EVI and NDVI from Landsat-8 data (Victor et al., 2015).

3. Results and discussion

3.1. Summer cultivated maize phenology and biophysical parameters

Phenology-wise biophysical parameters measured across the growing season of maize crop are presented in Table 2. Results revealed that the chlorophyll content increased continuously from 38.6% at the beginning of the crop growing season (V4 stage) up to 61.2% at the silking (R1 growth stage), and then decreased to 60.3% at the R2 stage (milking stage) i.e. the initiation of crop senescence. Similar to the chlorophyll content, the LAI values increased continuously from 1.22 at the V4 stage up to 6.87 at the R2 stage. It was observed that as the growing season progressed, the increase in the leaf area improved the ability of maize crop in assimilating CO_2. This is illustrated by the results of the net photosynthesis (P_n); in which, the increase in the LAI from 1.22 (V4) to 5.73 (V16) was associated with an increase in the magnitude of the net photosynthesis from 10.4 μmol m^{-2} s^{-1} (V4) to 18.2 μmol m^{-2} s^{-1} (V16). During this period, the maximum net photosynthesis was boosted by 75%. However, at R2 stage, it was reduced to 16.2 μmol m^{-2} s^{-1}. Hence, a reduction of 12% in the rate of photosynthesis was recorded at R2 stage compared to the V16 stage.

The results presented in Table 2 also indicated that maize crop exhibited a maximum transpiration rate (E) of 6.7 mmol m^{-2} s^{-1} at V16 with an increase of 45% compared to V4. While at R1, the value of E was drastically reduced by 45% compared to V16. However, there is an increase of 22% in the value of E from R1 stage (4.6 mmol m^{-2} s^{-1}) to R2 stage (5.6 mmol m^{-2} s^{-1}). The results also revealed that the stomatal conductance (gs) of the maize crop was directly correlated with the transpiration rate across the growth stages. For example, the gs increased from V4 (0.21 mmol m^{-2} s^{-1}) to V16 (0.39 mmol m^{-2} s^{-1}) by 85.71%, and slightly reduced to 0.34 mmol m^{-2} s^{-1} (i.e. 12.82%) at the R1 stage.

3.2. Seasonal patterns of micrometeorological data

The patterns of 8-day averaged EC measured photosynthetically active radiation (PAR), mean air temperature (°C), relative humidity (RH,%) and GPP_{EC} (g C m^{-2} d^{-1}) were assessed for the Landsat-8 date of pass (DOP), Table 3. The PAR exhibited highest values of 542 to 664 mol m^{-2} during hot conditions (i.e. late summer); while, the lowest values of 367 to 396 mol m^{-2} were observed during early winter.

As depicted in Fig. 2, the highest PAR values were observed during the dry season, which coincided with the early growth stage of maize crop (DOY- 241 to 249); where the recorded PAR was 665 mol m^{-2} at a mean air temperature of 43.25 °C. Subsequently, the value of the PAR decreased gradually throughout the study period. As depicted in Fig. 3, the measured LAI was inversely correlated with the EC measured PAR. At the early growth stage of maize (V2), the PAR value

Table 2 Maize crop measured biophysical parameters.

Growth stage	LAI	Chl (SPAD Values, %)	Pn (μmol m^{-2} s^{-1})	E (mmol m^{-2} s^{-1})	C_i (mmol m^{-2} s^{-1})	g_s (mmol m^{-2} s^{-1})
V4	1.22 ± 0.6	38.6 ± 4.6	10.4 ± 1.0	4.6 ± 0.4	180.3 ± 17.5	0.21 ± 0.04
V5	1.78 ± 0.9	48.2 ± 9.2	12.4 ± 0.2	3.54 ± 0.2	204.3 ± 13.5	0.28 ± 0.02
V7	3.01 ± 0.8	52.4 ± 7.8	13.5 ± 0.9	5.7 ± 0.1	229.4 ± 13.5	0.32 ± 0.01
V10	4.22 ± 1.1	54.2 ± 6.4	15.8 ± 0.5	6.2 ± 0.1	255.0 ± 19.1	0.37 ± 0.01
V12	4.91 ± 1.4	55.9 ± 11.6	14.2 ± 0.9	5.9 ± 0.3	286.7 ± 3.5	0.34 ± 0.01
V16	5.73 ± 1.2	58.6 ± 8.7	18.2 ± 1.1	6.7 ± 0.4	249.6 ± 16.9	0.39 ± 0.02
R1	6.54 ± 2.1	61.2 ± 6.2	17.4 ± 0.6	4.6 ± 0.2	248.3 ± 21.3	0.34 ± 0.03
R2	5.87 ± 2.4	60.3 ± 5.9	16.2 ± 0.9	5.6 ± 0.3	239.1 ± 19.5	0.38 ± 0.01

Chl = Chlorophyll content; LAI = leaf area index; Pn = net photosynthesis; E = rate of transpiration; Ci = Substomatal CO_2 concentration; gs = stomatal conductance.

Table 3 Eddy covariance flux tower measured PAR, temperature, relative humidity and GPP.

Growth stage	Eight day period (DOY)	PAR (mol m^{-2})	Temperature (°C)	RH (%)	GPP_{EC} (g C m^{-2} 8-d^{-1})
V2	241 to 248	664.72	43.25	13.91	−0.68
V4	249 to 256	624.21	44.50	11.92	11.78
V5	257 to 264	534.00	35.90	15.90	15.84
V7	265 to 272	542.19	38.20	18.88	19.22
V10	273 to 281	415.47	36.74	21.86	27.58
V12	282 to 288	451.68	32.15	25.83	38.69
V16	289 to 297	466.87	31.65	32.79	42.09
R1	298 to 304	367.28	29.18	35.77	35.82
R2	305 to 313	396.77	28.19	37.76	27.61

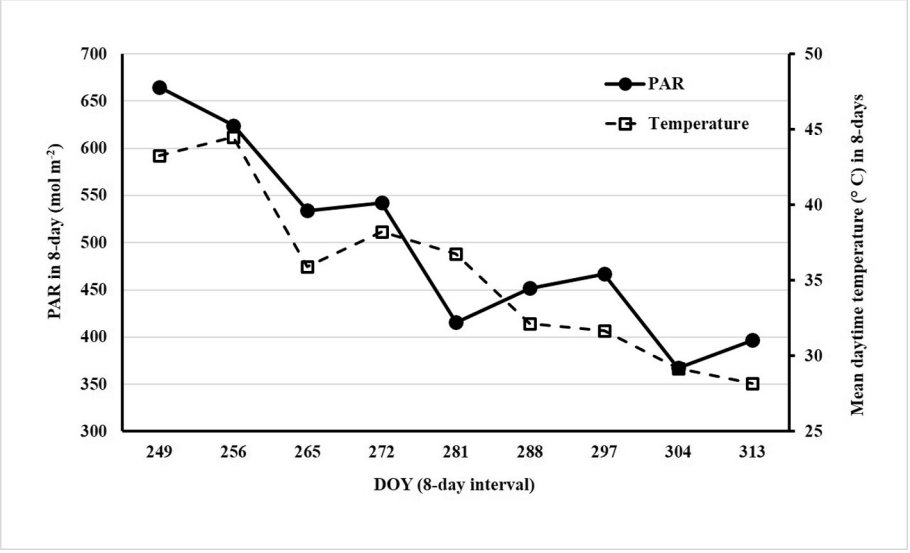

Figure 2 Temporal variation of EC system recorded PAR and mean daytime temperatures (8-day composites).

was maximum (645 mol m^{-2}), and the LAI was minimum (1.22 m^2 m^{-2}). On the other hand, the minimum PAR value (367.28 mol m^{-2}) was observed at the maximum LAI (6.54 m^2 m^{-2}).

3.3. Temporal analyses of the GPP_{EC}

Temporal dynamics of the GPP and the NEE measured by the EC flux tower (GPP_{EC} and NEE_{EC}) were assessed based on the growth stages of maize crop (Table 1), corresponding to Landsat-8 date of pass (DOP). Results revealed that changes in the NEE_{EC} of >1.0 g C m^2 d^{-1} took place immediately after crop emergence (Fig. 4). Both GPP_{EC} and NEE_{EC} increased gradually and reached their peak values at the V16 growth stage, and subsequently decreased at R1 and R2 stages. This clearly explained the physiological changes from vegetative to reproductive stages. The maximum value of maize GPP of 42.09 g C m^2 d^{-1} was recorded at V16 growth stage for the corresponding LAI value of 5.73 m^2 m^{-2}. Turner et al. (2003) reported relatively similar results of peak daily maize GPP of 28 g C m^2 d^{-1} at an LAI of 6 m^2 m^{-2}.

3.4. Seasonal dynamics of vegetation indices derived from Landsat-8 data

The seasonal dynamics of the NDVI, EVI and LSWI across the growing period of maize crop are provided in Fig. 5. It was observed that the NDVI, EVI and LSWI values increased with the developmental stages of the maize crop, and reached their peak values at the V12 growth stage (NDVI) and V16 stage (EVI and LSWI). At the V12 growth stage, the NDVI showed saturation status of NIR, which continued up to the R1 stage and subsequently declined after that. Significant variation in the values of vegetation indices was observed for NDVI and EVI, as indicated by their correlation with the GPP_{EC} (Fig. 6). The EVI showed the stronger significant linear correlation (at 5% level) with the GPP_{EC} ($R^2 = 0.86$ and $P = 0.0211$) than both NDVI ($R^2 = 0.81$ and $P = 0.0431$) and LSWI ($R^2 = 0.76$ and $P = 0.3262$). This can be attributed to the saturation of NDVI as the crop canopy approached its peak vegetative growth stage (V12); while, the EVI was more able to detect subtle increases in the density of crop canopy (Huete et al., 1997; Verma et al., 2005).

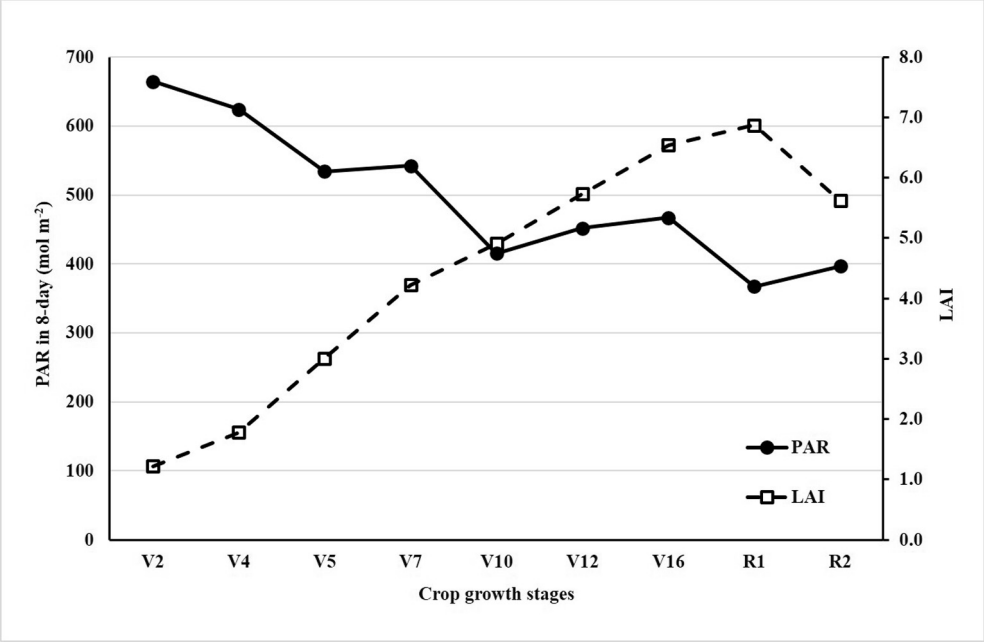

Figure 3 Variation of EC recorded PAR and ground measured LAI.

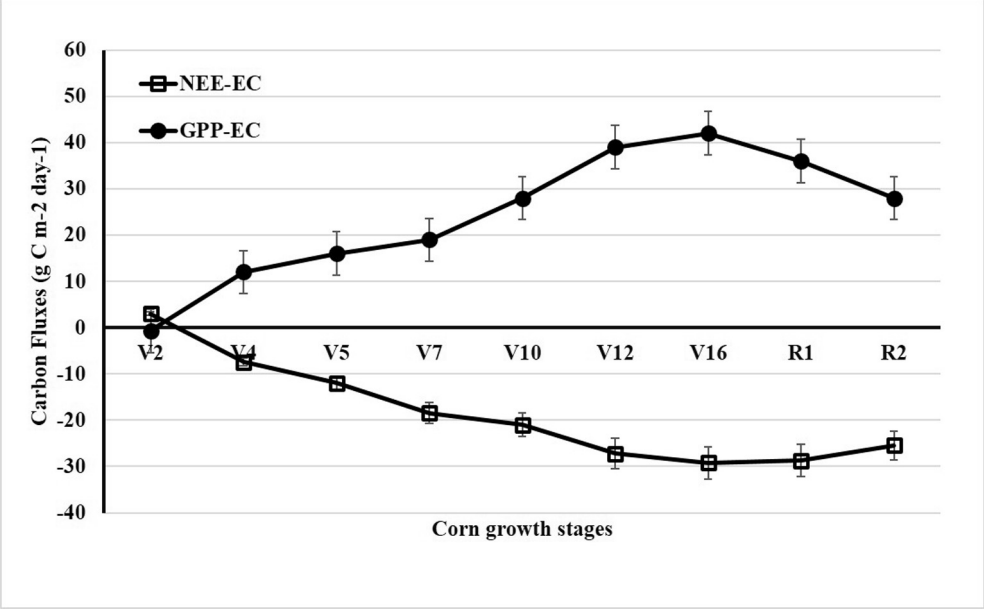

Figure 4 Temporal variation of EC estimated NEE and GPP.

3.5. Seasonal dynamics of the Vegetation Photosynthesis Model predicted GPP (GPP_{VPM})

Simulation of the VPM model was performed using NDVI and EVI vegetation indices derived from Landsat-8 surface reflectance data, temperature, and PAR for the study period (August to November 2015), Table 4. Pierson correlation between the GPP_{EC} and GPP_{VPM} (GPP_{EVI} and GPP_{NDVI}) was applied for the entire maize crop growth period along with the calculations of Root Mean Square Error (RMSE) and relative error (RE). The seasonal dynamics of the predicted GPP (GPP_{VPM}) agreed well with that estimated through the EC system (GPP_{EC}), regarding both phase and magnitude. As depicted in Fig. 7, the simple linear regression model showed high correlation between the GPP_{EC} with the GPP_{NDVI} ($R^2 = 0.93$ and $P = 0.0384$) and GPP_{EVI} ($R^2 = 0.96$ and $P = 0.0241$). The cumulative GPP_{EC} for the entire growth period of the center pivot irrigated maize crop was 1871 g C m^{-2} compared to the cumulative GPP_{EVI} of 1979 g C m^{-2} and GPP_{NDVI} of 1754 g C m^{-2}. The GPP_{EVI} was overestimated by 12.6% and the GPP_{NDVI} was underestimated by 19.7% compared to the GPP_{EC}. The recorded RE between the GPP_{EC}

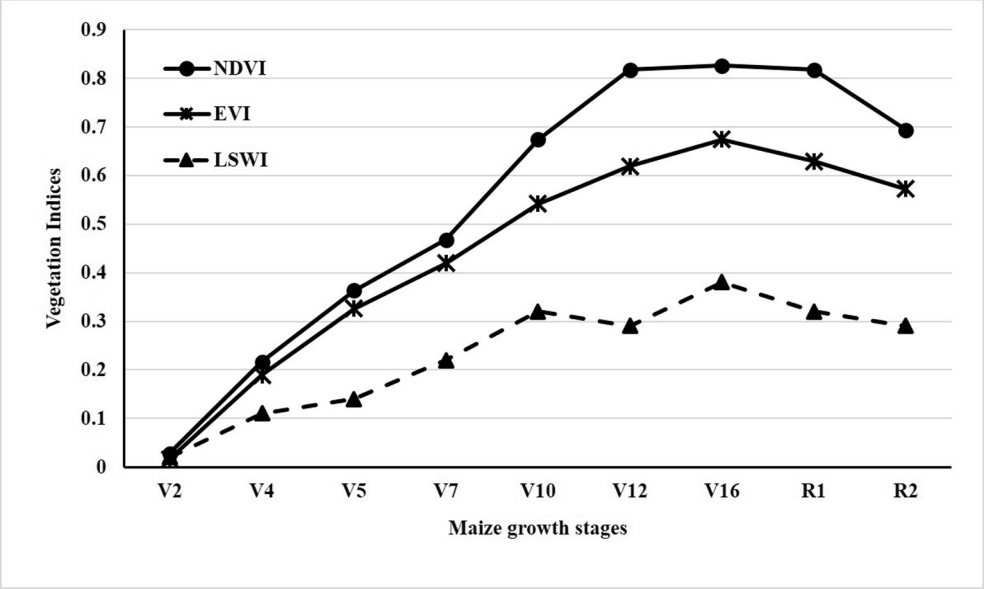

Figure 5 Dynamics of NDVI, EVI, and LSWI.

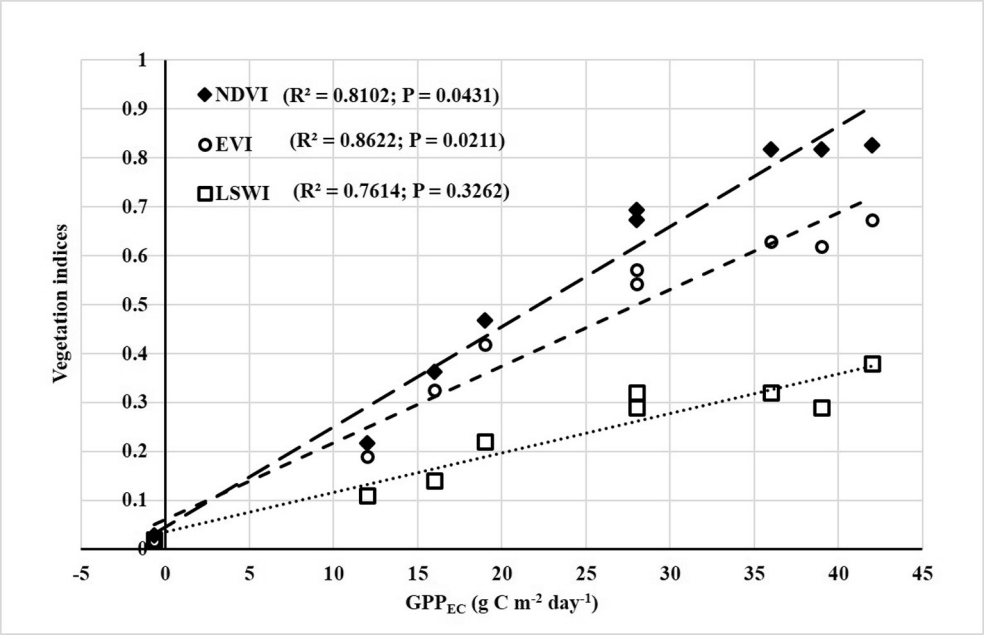

Figure 6 The relationship between the GPP_{EC} and vegetation indices (NDVI, EVI, and LSWI).

and GPP_{EVI} as well as GPP_{NDVI} was -6.22% and 5.76%, respectively.

The difference between the GPP_{EVI} and GPP_{NDVI} highlighted the limitations of each index. For example, the NDVI was observed to be more sensitive to the vegetation change, while the EVI showed a higher correlation with the LAI compared to the NDVI and did not show saturation with high LAI ($>6\ m^2\ m^{-2}$). This was evident in the studies of Huete et al. (2006) and Xiao et al. (2004a). In the case of phenology dynamics, the correlation between the GPP_{EC} and VIs (NDVI, EVI and LSWI) reached the peak at 55–60 days after sowing, i.e. the flowering and grain filling periods of maize crop in this study. The cumulative GPP_{EC} measured for maize crop ($1870\ g\ C\ m^2$) was in the range of the GPP values estimated for irrigated maize crop in previous studies, e.g. 1648 to $1743\ g\ C\ m^2$ (Kalfas et al., 2011) and $1567\ g\ C\ m^2$ (Wang et al., 2012).

Several studies on maize crop based on the eddy covariance technique have reported a large variation in GPP. Peak GPP values of this study were approximately $42\ g\ C\ m^{-2}\ d^{-1}$ (Fig. 4), which are much higher than peak GPP values ($\sim 15\ g\ C\ m^{-2}\ d^{-1}$) at three maize sites in China (Yan et al., 2009; Lei and Yang, 2010; Wang et al., 2010b; Wu et al., 2010c) and moderately higher than peak GPP values ($\sim 25\ g\ C\ m^{-2}\ d^{-1}$) at two maize sites in France (Beziat et al., 2009; Stella et al., 2009). The GPP_{EVI} was significantly higher

Table 4 Eddy covariance flux tower measured and Vegetation Photosynthesis Model (VPM) derived gross primary production (GPP).

Growth Stage	GPP_{NDVI}		GPP_{EVI}		GPP_{EC}	
	g C m^{-2} d^{-1}	g C m^{-2} 8-d^{-1}	g C m^{-2} d^{-1}	g C m^{-2} 8-d^{-1}	g C m^{-2} d^{-1}	g C m^{-2} 8-d^{-1}
V2	−0.77	−6.58	−0.02	−0.17	−0.68	−5.78
V4	12.30	104.55	13.99	118.88	12.18	103.53
V5	15.58	132.43	17.98	152.85	16.17	137.45
V7	17.63	149.86	19.98	169.84	18.94	160.99
V10	24.60	209.11	28.97	246.28	27.91	237.24
V12	34.93	296.91	40.97	348.27	39.64	336.94
V16	39.90	339.15	43.96	373.67	42.14	358.19
R1	36.80	312.8	37.01	314.62	35.72	303.62
R2	25.42	216.07	29.97	254.77	28.06	238.51
Cumulative GPP		1754.28		1979.01		1870.68
RMSE		19.71		12.55		
RE%		−6.22		5.79		

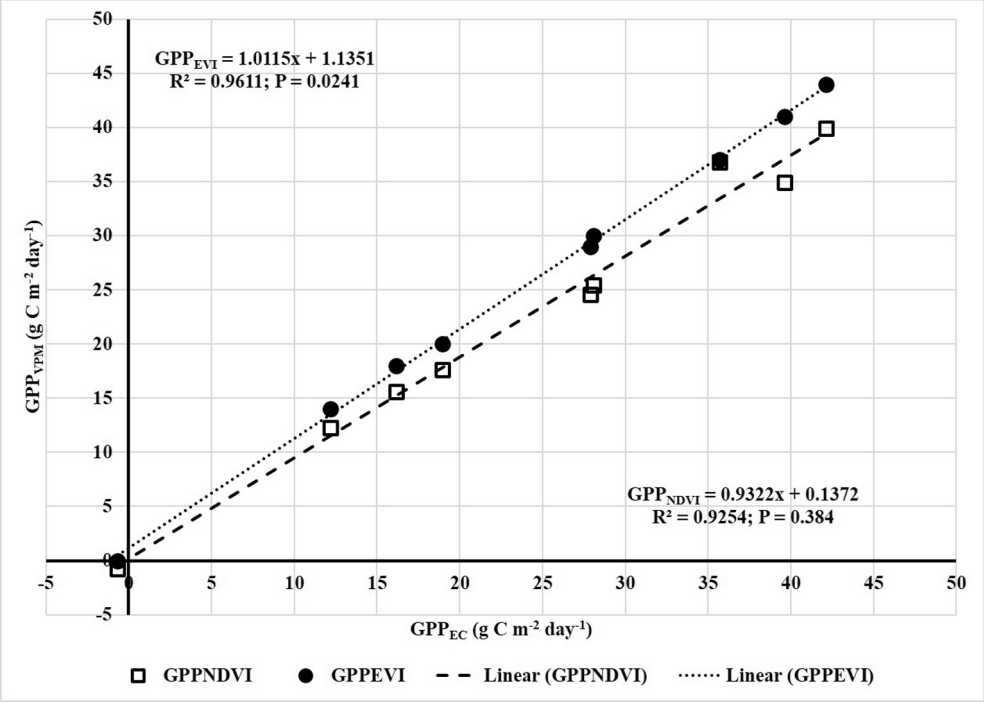

Figure 7 The relationship between the GPP_{EC} and GPP_{VPM} across the study period.

than the GPP_{EC} (R^2 = 0.96, P = 0.0241 and RMSE = 12.6%). While, the GPP_{NDVI} was significantly lower than the GPP_{EC} (R^2 = 0.93, P = 0.0384 and RMSE = 19.7%). In a previous study, the VPM was applied to two maize sites in China, and the GPP_{VPM} tracked well with the seasonal dynamics of GPP_{EC} (Yan et al., 2009; Wang et al., 2010b).

4. Conclusion

In this study, the GPP of maize crop, cultivated during August to November 2015 in the eastern region of Saudi Arabia, was estimated using the VPM model based on a Landsat-8 reflectance (GPP_{VPM}) as well as the meteorological data provided by the Eddy Covariance (EC) system (GPP_{EC}). The following conclusions are inferred from the study:

- The GPP_{EVI} was significantly higher than the GPP_{EC} (R^2 = 0.96, P = 0.0241 and RMSE = 12.6%), while, the GPP_{NDVI} was significantly lower than the GPP_{EC} (R^2 = 0.93, P = 0.0384 and RMSE = 19.7%).
- The VPM model provided accurate estimation of the GPP with a relative error of about 6% compared to the EC measured GPP.
- The VPM model demonstrated the potentiality of estimating the GPP of cropland ecosystems using Landsat-8 imagery.

Acknowledgements

This project was financially supported by King Saud University, Vice Deanship of Research Chairs. The unstinted cooperation and support extended by Mr. Jack King and Mr. Alan King and their team of Todhia Arable Farm are gratefully acknowledged.

References

Asrar, G., Myneni, R.B., Choudhury, B.J., 1992. Spatial heterogeneity in vegetation canopies and remote sensing of absorbed photosynthetically active radiation: a modelling study. Remote Sens. Environ. 41, 85–103.

Baker, J., Griffis, T., 2005. Examining strategies to improve the carbon balance of corn/soybean agriculture using eddy covariance and mass balance techniques. Agric. Forest Meteorol. 128, 163–177.

Baldocchi, D., Meyers, T., 1998. On using eco-physiological, micrometeorological and biogeochemical theory to evaluate carbon dioxide, water vapor and trace gas fluxes over vegetation: a perspective. Agric. Forest Meteorol. 90, 1–25.

Beziat, P., Ceschia, E., Dedieu, G., 2009. Carbon balance of a three crop succession over two cropland sites in South West France. Agric. Forest Meteorol. 149, 1628–1645.

Crafts-Brandner, S.J., Salvucci, M.E., 2002. Sensitivity of photosynthesis in a C4 plant, maize, to heat stress. Plant Physiol. 129 (4), 1773–1780.

DeFries, R., 2008. Terrestrial vegetation in the coupled human-earth system: contributions of remote sensing. Annu. Rev. Environ. Resour. 33, 369–390.

Desai, A.R., Noormets, A., Bolstad, P.V., Chen, J., et al, 2008. Influence of vegetation and seasonal forcing on carbon dioxide fluxes across the Upper Midwest, USA: implications for regional scaling. Agric. Forest Meteorol. 148 (2), 288–308.

Falge, E., Baldocchi, D., Tenhunen, J., Aubinet, M., Bakwin, P., Berbigier, P., Bernhofer, C., Burba, G., Clement, R., Davis, K.J., 2002. Seasonality of ecosystem respiration and gross primary production as derived from FLUXNET measurements. Agric. Forest Meteorol. 113, 53–74.

Gitelson, A.A., Vina, A., Masek, J.G., Verma, S.B., Suyker, A.E., 2008. Synoptic monitoring of gross primary productivity of maize using Landsat data. IEEE Geosci. Remote Sen. Lett. 5 (2), 133–137.

Goulden, M.L., Daube, B.C., Fan, S.M., Sutton, D.J., Bazzaz, A., Munger, J.W., Wofsy, S.C., 1997. Physiological responses of a black spruce forest to weather. J. Geophys. Res. D: Atmos. 102, 28987–28996.

Gwathmey, C.O., Tyler, D.D., Yin, X., 2010. Prospects for monitoring cotton crop maturity with Normalized Difference Vegetation Index. Agron. J. 102 (5), 1352–1360.

Huete, A.R., Liu, H.Q., Batchily, K., van Leeuwen, W.J.D., 1997. A comparison of vegetation indices over a global set of TM images for EOS-MODIS. Remote Sens. Environ. 59, 440–451.

Huete, A., Didan, K., Miura, T., Rodriguez, E.P., Gao, X., Ferreira, L.G., 2002. Overview of the radiometric and biophysical performance of the MODIS vegetation indices. Remote Sens. Environ. 83, 195–213.

Huete, A.R., Didan, K., Shimabukuro, Y.E., Ratana, P., Saleska, S. R., Hutyra, L.R., Fitzjarrald, D., Yang, W., Nemani, R.R., Myneni, R., 2006. Amazon rainforests green–up with sunlight in dry season. Geophys. Res. Lett. 33, L 06405. http://dx.doi.org/10.1029/2005GL025583.

Hunt Jr., E.R., Kelly, R.D., Smith, W.K., Fahnestock, J.T., Welker, J. M., Reiners, W.A., 2004. Estimation of carbon sequestration by combining remote sensing and net ecosystem exchange data for Northern Mixed-Grass Prairie and Sagebrush-Steppe Ecosystems. Environ. Manage. 33, S432–S441.

Kalfas, J.L., Xiao, X., Vanegas, D.X., Verma, S.B., Suyker, A.E., 2011. Modeling gross primary production of irrigated and rain-fed maize using MODIS imagery and CO_2 flux tower data. Agric. Forest Meteorol. 151 (12), 514–1528.

Kang, X., Hao, Y., Cui, X., Chen, H., Huang, S., Du, Y., Li, W., Kardol, P., Xiao, X., Cui, L., 2016. Variability and changes in climate, phenology and gross primary production of an alpine wetland ecosystem. Remote Sens. 8, 391. http://dx.doi.org/10.3390/rs8050391.

Kim, S.H., Gitz, D.C., Sicherb, R.C., Baker, J.T., Timlin, D.J., Reddy, V.R., 2007. Temperature dependence of growth, development, and photosynthesis in maize under elevated CO_2. Environ. Exp. Bot. 61 (3), 224–236.

Lei, H., Yang, D., 2010. Interannual and seasonal variability in evapotranspiration and energy partitioning over an irrigated cropland in the North China Plain. Agric. Forest Meteorol. 150 (4), 581–589.

Li, Z.Q., Yu, G.R., Xiao, X.M., Li, Y.N., Zhao, X.Q., Ren, C.Y., Zhang, L.M., Fu, Y.L., 2007. Modeling gross primary production of alpine ecosystems in the Tibetan Plateau using MODIS images and climate data. Remote Sens. Environ. 107 (3), 510–519.

Osmond, B., Ananyev, G., Berry, J., Langdon, C., Kolber, Z., Lin, G. H., et al, 2004. Changing the way we think about global change research: Scaling up in experimental ecosystem science. Global Change Biol. 10, 393–407.

Pan, S., Tian, H., Dangal, S.R.S., Ouyang, Z., Tao, B., Ren, W., Lu, C., Running, S., 2014. Modeling and monitoring terrestrial primary production in a changing global environment: toward a multiscale synthesis of observation and simulation. Adv. Meteorol., 17 (Article ID 965936)

Pingintha, N., Leclerc, M.Y., Beasley Jr., J.P., Durden, D., Zhang, G., Senthong, C., Rowland, D., 2010. Hysteresis response of daytime net ecosystem exchange during drought. Biogeoscience 7, 1159–1170.

Raich, J.W., Rastetter, E.B., Melillo, J.M., Kicklighter, D.W., Steudler, P.A., Peterson, B.J., Grace, A.L., Moore, B., Vorosmarty, C.J., 1991. Potential net primary productivity in South America: application of a global model. Ecol. Appl. 1 (4), 399–429.

Sakamoto, T., Gitelson, A.A., Wardlow, B.D., Verma, S.B., Suyker, A.E., 2011. Estimating daily gross primary production of maize based only on MODIS WDRVI and shortwave radiation data. Remote Sens. Environ. 115, 3091–3101.

Shim, C., Jiyoun, Hong, Jinkyu, Hong, Kim, Y., Kang, M., Thakuri, B.M., Kim, Y., Chun, J., 2014. Evaluation of MODIS GPP over a complex ecosystem in East Asia: A case study at Gwangneung flux tower in Korea. Adv. Space Res. 54, 2296–2308.

Silva, F.B., Shimabukuro, Y.E., Aragao, L.E.O.C., Anderson, Pereira, Cardozo, Arai, 2013. Large-scale heterogeneity of Amazonian phenology revealed from 26 yearlong AVHRR/ NDVI time-series Environ. Res. Lett. 8, 024011.

Sims, D.A., Rahman, A.F., Cordova, V.D., El-Masri, B.Z., Baldocchi, D.D., Bolstad, P.V., Flanagan, L.B., Goldstein, A.H., Hollinger, D.Y., Misson, L., Monson, R.K., Oechel, W.C., Schmid, H.P., Wofsy, S.C., Xu, L., 2008. A new model of gross primary productivity for North American ecosystems based solely on the enhanced vegetation index and land surface temperature from MODIS. Remote Sens. Environ. 112 (4), 1633–1646.

Souza, M.C., Biudes, M.S., Danelichen, V.H., Machado, N.G., De-Musis, C.R., Vourlitis, G.L., Nogueira, J.D., 2014. Estimation of gross primary production of the Amazon-Cerrado transitional forest by remote sensing techniques. Revista Bras. Meteorol. 29 (1), 1–24.

Stella, P., Lamaud, E., Brunet, Y., Bonnefond, J.M., Loustau, D., Irvine, M., 2009. Simultaneous measurements of CO_2 and water exchanges over three agroecosystems in South-West France.

Biogeoscience 6, 2957–2971. http://dx.doi.org/10.5194/bg-6-2957-2009.

Tang, X., Li, H., Griffis, T.J., Xu, X., Ding, Z., Liu, G., 2015. Tracking ecosystem water use efficiency of cropland by exclusive use of MODIS EVI data. Remote Sens. 7, 11016–11035.

Tucker, C.J., 1979. Red and photographic infrared linear combinations for monitoring vegetation. Remote Sens. Environ. 8, 127–150.

Turner, D.P., Ritts, W.D., Cohen, W.B., Gower, S.T., Zhao, M., Running, S.W., Wofsy, S.C., Urbanski, S., Dunn, A.L., Munger, J. W., 2003. Scaling gross primary production (GPP) over boreal and deciduous forest landscapes in support of MODIS GPP product validation. Remote Sens. Environ. 88, 256–270.

USGS, 2015. Using the USGS Landsat 8 Product. Accessed on 17 August 2015 from http://landsat.usgs.gov/Landsat8_Using_Product.php.

Vashum, K.T., Jayakumar, S., 2012. Methods to estimate above-ground biomass and carbon stock in natural forests – a review. J. Ecosyst. Ecogr. 2, 116. http://dx.doi.org/10.4172/2157-7625.1000116.

Verma, S.B., Walters, D.T., Knops, J.M., Arkebauer, T.J., Suyker, A. E., Burba, G.G., et al, 2005. Annual carbon dioxide exchange in irrigated and rainfed maize-based agroecosystems. Agric. Forest Meteorol. 131, 77–96. http://dx.doi.org/10.1016/j.agrformet.2005.05.003.

Victor, H.M.D., Marcelo, S.B., Maisa, C.S.V., Nadja, G.M., Raphael, S.R.G., George, L.V., Joses, N., 2015. Estimating of gross primary production in an Amazon-Cerrado transitional forest using MODIS and Landsat imagery. Ann. Brazilian Acad. Sci. 87 (3), 1545–1564.

Wagle, P., Xiao, X., Suyker, A., 2015. Estimation and analysis of gross primary production of soybean under various management practices and drought conditions. ISPRS J. Photogramm. Remote Sens. 99, 70–83.

Wang, Z., Xiao, X., Yan, X., 2010. Modeling gross primary production of maize cropland and degraded grassland in northeastern China. Agric. Forest Meteorol. 150 (9), 1160–1167.

Wang, X., Ma, M., Huang, G., Veroustraete, F., Zhang, Z., Song, Y., Tan, J., 2012. Vegetation primary production estimation at maize and alpine meadow over the Heihe River Basin, China. Int. J. Appl. Earth Obs. Geoinf. 17, 94–101.

Wohlfahrt, G., Anfang, C., Bahn, M., Haslwanter, A., Newesely, C., Schmitt, M., Drosler, M., Pfadenhaeur, J., Cernusca, A., 2005. Quantifying nighttime ecosystem respiration of a meadow using eddy covariance, chambers and modeling. Agric. Forest Meteorol. 128, 141–162.

Wu, W.X., Wang, S.Q., Xiao, X.M., Yu, G.R., Fu, Y.L., Hao, Y.B., 2008. Modeling gross primary production of a temperate grassland ecosystem in Inner Mongolia, China, using MODIS imagery and climate data. Sci. China Ser. D-Earth Sci. 51 (10), 1501–1512.

Wu, C.Y., Han, X.Z., Ni, J.S., Niu, Z., Huang, W.J., 2010. Estimation of gross primary production in wheat from in situ measurements. Int. J. Appl. Earth Obs. 12 (3), 183–189.

Xiao, X., Hollinger, D., Aber, J., Goltz, M., Eric, A.D., Zhang, Q., Moore, B.I.I.I., 2004a. Satellite-based modeling of gross primary production in an evergreen needle leaf forest. Remote Sens. Environ. 89, 519–534.

Xiao, X., Zhang, Q., Braswell, B., Urbanski, S., Boles, S., Wofsy, S., et al, 2004b. Modeling gross primary production of temperate deciduous broadleaf forest using satellite images and climate data. Remote Sens. Environ. 91, 256–270.

Xiao, X., Zhang, Q., Hollinger, D., Aber, J., Moore, B., 2005a. Modeling gross primary production of an evergreen needleleaf forest using MODIS and climate data. Ecol. Appl. 15 (3), 954–969.

Xiao, X., Zhang, Q., Saleska, S., Hutyra, L., De Camargo, P., Wofsy, S., Frolking, S., Boles, S., Keller, M., Moore, B., 2005b. Satellite-based modeling of gross primary production in a seasonally moist tropical evergreen forest. Remote Sens. Environ. 94 (1), 105–122.

Xiao, X., Boles, S., Liu, J.Y., Zhuang, D.F., Frolking, S., Li, C.S., Salas, W., Moore, B., 2005c. Mapping paddy rice agriculture in southern China using multi-temporal MODIS images. Remote Sens. Environ. 95 (4), 480–492.

Yan, H.M., Fu, Y.L., Xiao, X.M., Huang, H.Q., He, H.L., Ediger, L., 2009. Modeling gross primary productivity for winter wheat-maize double cropping system using MODIS time series and CO_2 eddy flux tower data. Agric. Ecosyst. Environ. 129 (4), 391–400.

Zhao, M., Running, S.W., 2010. Drought-induced reduction in global terrestrial net primary production from 2000 through 2009. Science 329 (5994), 940–943.